Journal of Applied Polymer Science

Influence of diaminobenzoyl-functionalized multiwalled carbon nanotubes on the nonisothermal curing kinetics, dynamic mechanical properties, and thermal conductivity of epoxy–anhydride composites

Uraiwan Pongsa, Chavakorn Samthong, Piyasan Praserthdam, Anongnat Somwangthanaroj
Department of Chemical Engineering, Faculty of Engineering, Chulalongkorn University, Bangkok 10330, Thailand
Correspondence to: A. Somwangthanaroj (E-mail: anongnat.s@chula.ac.th)

ABSTRACT: To obtain advanced materials with a high thermal dissipation, the addition of multiwalled carbon nanotubes containing diverse functionality groups, that is, as-received multiwalled carbon nanotubes (AS-MWCNTs) and diaminobenzoyl multiwalled carbon nanotubes (DA-MWCNTs), to epoxy–anhydride composites was accomplished. According to nonisothermal differential scanning calorimetry analysis, the reactive functional groups present on the surfaces of the AS-MWCNTs and DA-MWCNTs accelerated the nucleophilic addition reaction of epoxy composites. Because of the difference in the reactivities of these functional groups toward epoxy groups, the distinction of fractional conversion and the reaction rate of the curing process were remarkably evident at the early stage. A suitable kinetic model was effectively elucidated with the Málek approach. The curing kinetics could best be described by a two-parameter autocatalytic model as a truncated Šesták–Berggren model. The DA-MWCNTs achieved effective load transfer and active heat conductive pathways; this resulted in good dynamic mechanical and thermal properties. As a result, the diglycidyl ether of bisphenol A/DA-MWCNTs constituted an effective system with enhanced heat dissipation of materials for electronic applications.
 J. Appl. Polym. Sci. **2016**, *133*, 43567.

KEYWORDS: adhesives; composites; crosslinking; differential scanning calorimetry (DSC)

Received 1 May 2015; accepted 19 February 2016
DOI: 10.1002/app.43567

INTRODUCTION

The epoxy adhesive has become an interesting thermosetting polymer for many diverse engineering applications requiring high reliability and endurance, including applications in the electronics, automotive, aeronautics, and construction industries. This has occurred because of its outstanding adhesive strength to a large variety of materials, long working time, good mechanical strength, and solvent and moisture resistances. Additionally, the final performance of epoxy adhesive can be easily controlled by the variation of the curing agent and catalyst and the curing conditions.[1] However, neat epoxy resin still has several drawbacks for use in electronics packaging, in particular, its low heat dissipation, which leads to stress cracking as a result of heat accumulation. Therefore, the thermal conductivity of epoxy needs to be improved.

Many researchers have made noteworthy efforts to manipulate the properties of epoxy by the addition of highly capable fillers into the matrix.[2–7] Currently, multiwalled carbon nanotubes (MWCNTs) have become intensively attractive as potential reinforcing materials in the polymer nanocomposites because of their exceptional characteristics, including their extremely high aspect ratio (>1000), high thermal conductivity (3000 W m^{-1} K^{-1} at room temperature), high tensile strength (50–200 MPa), high Young's modulus (~1.2 TPa), and ultralight weight.[8–11] Likewise, the commercial-scale production of high-purity and low-cost MWCNTs has been already accomplished.[12,13] Hence, polymer/carbon nanotube (CNT) nanocomposites have been suggested for the development of advanced materials with high thermal dissipation. Unfortunately, the optimal properties of polymer/CNT nanocomposites are far from what we expected because the incorporation of CNTs into the polymer matrix results in two critical problems, that is, the poor dispersion of entangled CNTs in organic solvents and polymers and weak interfacial interaction between the CNTs and polymer matrix because of their high specific surface area and strong van der Waals forces between the individual tubes. The modification of the surface chemistry of CNTs is, therefore, of special import for obtaining processing and probable applications for them in polymer nanocomposites.[14–17]

The noncovalent modification has been carried out to increase the dispersibility of CNTs in organic solvents and the polymer matrix because the conjugated system of CNTs was undisrupted. The polymer wrapping technique was achieved by the covering

of the individual CNTs with the polymer through van der Waals interactions and π–π stacking between the aromatics rings of the polymer chains and the CNT surface; this prevented their aggregation.[18] Furthermore, the physical adsorption of the surfactant can reduce the rebundling of the CNTs because the electrostatic/steric repulsive forces of the surfactant overcome the van der Waals interactions.[19] However, the main disadvantage of noncovalent modification is that the interfacial interaction between the CNTs and polymer matrix is inherently weak and unstable. Therefore, the covalent modification of CNTs is an alternative method for the better dispersion of CNTs. Generally, CNTs are intrinsically inert because of the nature of the aromatic structure on the surface. Thus, the introduction of reactive functional groups on their surface has always been carried out under harsh reaction conditions, and this causes serious structural damage and deterioration of the properties of the nanocomposites. For example, MWCNTs functionalized via oxidative acid treatment with various chemical oxidants (e.g., HNO_3, H_2SO_4, $KMnO_4$) have shown increased concentrations of oxygen-containing functional groups in conjunction with unwanted sidewall damage and nanotube shortening, which could disturb the π-electron cloud.[5–7,20] Also, many separation and purification steps of synthesized CNTs were unavoidably necessary to eliminate residual chemical reagents and impurities. From this reason, the chemical functionalization method with minimum damage on the molecular framework of CNTs and a simple synthesis protocol is expected to be a new challenging technique for preserving the strength improvement of CNT nanocomposites.

Friedel–Crafts acylation is a promising and effective approach for the purification and functionalization of nanotubes in a one-pot procedure.[21–25] Furthermore, this reaction can be carried out to functionalize other carbon-based materials, for example, graphene,[26] nanodiamonds,[27] and fullerene,[28] for the preparation of polymer nanocomposites. MWCNTs are functionalized via an electrophilic aromatic substitution reaction, in which the electrophile is a carbocation, in a mild poly(phosphoric acid) (PPA)/phosphorus pentoxide (P_2O_5) medium without damage to the CNTs. This maintains the unique properties of the MWCNTs and enhances the good dispersibility and better interfacial interaction between the CNTs and the polymer matrix. This outcome can offer great versatility in many applications.

There is still one topic concerning the preparation of nanocomposites containing functionalized MWCNTs. In the curing process of unfilled epoxy resin, the reactive groups of the curing agents directly couple with the oxirane rings of the epoxy matrix via a ring-opening reaction under high-temperature conditions; therefore, the curing behavior and final properties for the neat epoxy system are not very difficult to manipulate. In case of MWCNT-filled epoxy nanocomposites, it is possible that the functionalities on the surfaces of the untreated and treated MWCNTs can affect the curing mechanism on heating (nonisothermal conditions); this results in a more complicated curing reaction. In our previous studies,[29,30] we found that the grafting of functional groups on MWCNT surface significantly accelerated the curing reaction of epoxy nanocomposites; however, the curing parameters, including the reaction order, have still not been deeply examined. Consequently, the main aim of this study was to investigate the effect of the functionalization of diaminobenzoyl moieties on the MWCNT surface [diaminobenzoyl multiwalled carbon nanotubes (DA-MWCNTs)] and to compare them with untreated as-received multiwalled carbon nanotubes (AS-MWCNTs) with respect to the curing behavior, mechanical and thermal properties, and thermal conductivity of the epoxy–anhydride nanocomposites. The surface chemistry of the MWCNTs was analyzed with X-ray photoelectron spectroscopy (XPS), and the MWCNT dispersion in the epoxy matrix was observed by scanning electron microscopy (SEM). Furthermore, the curing kinetics was also examined with differential scanning calorimetry (DSC) in nonisothermal mode along with the theoretical models to elucidate the curing parameters.

EXPERIMENTAL

Materials

Diglycidyl ether of bisphenol A with an epoxide equivalent weight (EEW) of 189 g/equiv purchased from Dow Chemical Co. was used as epoxy-based polymer (EP). Hexahydro-4-methylphthalic anhydride (96%) was used as the curing agent. AS-MWCNTs were obtained from Chengdu Organic Chemicals Co. (Chinese Academy of Sciences). These nanotubes were further functionalized with 3,5-diaminobenzoic acid via a direct Friedel–Crafts acylation in a mild PPA/P_2O_5 medium to obtain the DA-MWCNTs. The processing conditions of the functionalization were described in more detail in our previous articles.[29,30] The AS-MWCNTs and DA-MWCNTs were used as filler in this study.

Composite Fabrication

An amount of functionalized MWCNTs at a filler content of 0.3 vol % was first sonicated in the curing agent, which acted as a dispersing agent because of its low viscosity, for 30 min to enhance the dispersion of the fillers. The epoxy resin was then added to the mixture and stirred until it was homogeneous. The catalyst was dissolved in the mixture by ultrasonication for 30 min. The resulting mixture was degassed in a vacuum oven and was then transferred to an aluminum mold. A small quantity of fresh sample was taken for DSC analysis. After it was cured at an elevated temperature, the sample was slowly cooled down to room temperature. The mold was peeled off, and the sample was polished for further investigation.

Characterization

XPS was used to evaluate the surface chemistry of the MWCNTs on the uppermost surface about 10–15 nm in depth. XPS analysis was performed with an AMICUS photoelectron spectrometer equipped with an Mg Kα X-ray as a primary excitation and KRATOS VISION2 software. The XPS survey spectra were collected at binding energies of 0–1000 eV with a step size of 1 eV. To examine more information about the chemical bonds of the functional groups on the topmost surface of the samples, the high-resolution photoelectron peaks were considered. The deconvolution of the high-resolution XPS peaks was accomplished with a nonlinear curve-fitting program (Origin Pro 8.1 software). The Shirley method was chosen to create an XPS baseline, and we subtracted this before quantification. Afterward, the curve-fitting procedure was performed with an

amplitude version of a Gaussian peak function fitting program; this was repeated until an optimized peak shape was attained.

DSC was conducted to elucidate how the presence of MWCNTs decorated with different functional groups in the epoxy composites influenced their curing characteristics through a comparison with the neat epoxy resin. Nonisothermal experiments were performed with DSC TA Instruments model 2910 DSC at different heating rates (βs) of 3, 5, 10, and 20 °C min^{-1}. Samples of fresh epoxy mixtures of approximately 5 mg were sealed into aluminum pans and heated up to 350 °C from room temperature under a nitrogen atmosphere at a flow rate of 50 mL min^{-1}. DSC data were then used to determine the degree of curing (α), reaction rate ($d\alpha/dt$), and kinetic parameters.

The dispersion of carbon nanotubes in the epoxy matrix was observed by a scanning electron microscope (Hitachi S-3400). The cured samples were fractured in liquid nitrogen and subsequently coated with a thin layer of gold before SEM measurement.

The dynamic mechanical properties of the epoxy composites were investigated with a Pyris Diamond DMA instrument (Perkin Elmer). Bending mode was used at a frequency of 1 Hz for all of the samples. The samples were heated from room temperature to 200 °C at a β of 5 °C min^{-1} under an N_2 atmosphere.

Laser-flash thermal conductivity measurements for the epoxy matrix and their composites were accomplished in this study. The thermal diffusivity of the samples was measured with an LFA 1000 laser flash (Netzsch, Germany). The sample surface was irradiated with a very short laser pulse, and the temperature rise was measured on the opposite side of the sample; we then used this to calculate the thermal diffusivity. The specific heat capacity (C_p) was measured with DSC (PerkinElmer Pyris Diamond differential scanning calorimeter). In addition, the bulk density of the specimen was measured by water displacement.

RESULTS AND DISCUSSION

Surface Chemistry of the Functionalized MWCNTs

It is well recognized that the functionalities on the filler surface had a substantial influence on the reactivity divergence, frequently altering the curing characteristics and leading to changes in the final properties of the reinforced epoxy composites. Consequently, XPS analysis was applied to distinguish the chemical compositions of the uppermost surface of the MWCNTs before use. The XPS survey spectra of the AS-MWCNTs and DA-MWCNTs are displayed in Figure 1. The major peaks of the C1s and O1s photoelectrons were observed in all of the survey spectra at about 285 and 534 eV, respectively.[31,32] This result revealed that the surface of the unmodified MWCNTs had a small amount of oxygen-containing functionalities, which were unintentionally produced from carbon impurities during the purification of the as-produced MWCNTs, for example, during the use of strong oxidizing agents, such as concentrated acids.[33] In comparison with the AS-MWCNTs, the intensity of the C1s peak decreased noticeably, whereas the O1s peak increased for the DA-MWCNTs. This was due to the fact that during the functionalization, the carbon atoms were bothered, and this generated additional defects in which the ring structure of the MWCNTs was opened and the oxygen-containing functionalizing reactants were

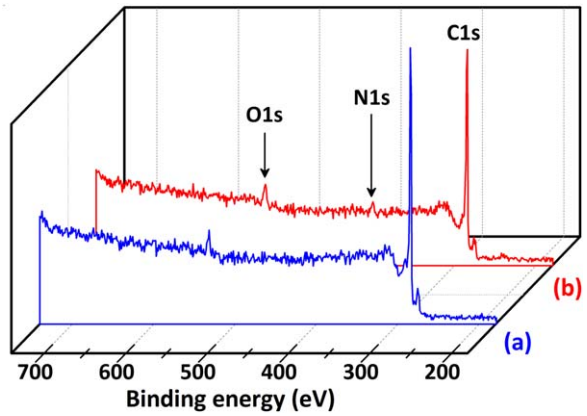

Figure 1. XPS survey spectra of the (a) AS-MWCNTs and (b) DA-MWCNTs. [Color figure can be viewed in the online issue, which is available at wileyonlinelibrary.com.]

attached and stabilized in the MWCNTs' structures. As a result, the O/C ratio of the DA-MWCNTs (0.20%) was two times that of the AS-MWCNTs (0.11%). Moreover, the N1s peak was observed only in the XPS survey spectrum of the DA-MWCNTs at about 400.2 eV; this was attributed to a primary amine bonded with C═C bond and indicated the effective grafting of diaminobenzoyl moieties on their surface.[34,35] On the basis of the known chemical structure and the atomic composition of the grafted functional group, the degree of functionalization of the diaminobenzoyl moieties on the MWCNT surface was calculated to be approximately 3.37%.

To clarify the functional groups and the chemical bonding on the surface of MWCNTs, curve fitting of the characteristic peaks in the XPS survey spectra was accomplished. The high-resolution XPS spectra for the C1s region were deconvoluted into many individual peaks, as demonstrated in Figure 2, which represents the types of carbon bonding in the nanotube structure. There is general agreement in the literature on the assignment of the peaks in the C1s deconvolution.[32,36–38] The main peaks of the sp^2-hybridized graphite-like carbon atoms (C═C) and the sp^3-hybridized diamond-like carbon atoms (C—C), or the defects on the nanotube structure, were found at 284.2–284.5 and 285.2–285.5 eV, respectively. Various functionalities on the MWCNT surfaces were observed as smaller peaks at 286.1–286.3 eV (C—O), 286.6 eV (C—NH_2), 287.4–287.6 eV (C═O), and 288.1 eV (COOH). In addition, the peak assigned to the π–π^* transition in aromatic rings was observed at 290.8 eV. From the results, we found that the relative contents of the different chemical states of carbon significantly changed after the surface modification. In the acylation of the MWCNTs, the —COOH groups of diamiobenzoic acid were directly reacted with the defective sp^2 C—H groups on the surface of MWCNTs for the electrophilic substitution; this led to a decrease in the C═C structure and an increase in the C—C structure in the DA-MWCNT samples. Furthermore, the XPS spectrum of the acylated MWCNTs showed an increase in the concentration of C═O as a result of the newly formed carbonyl linkages via Friedel–Crafts acylation and the detection of C—NH bonds; this confirmed the presence of diaminobenzoyl moieties on the surface of the MWCNTs.

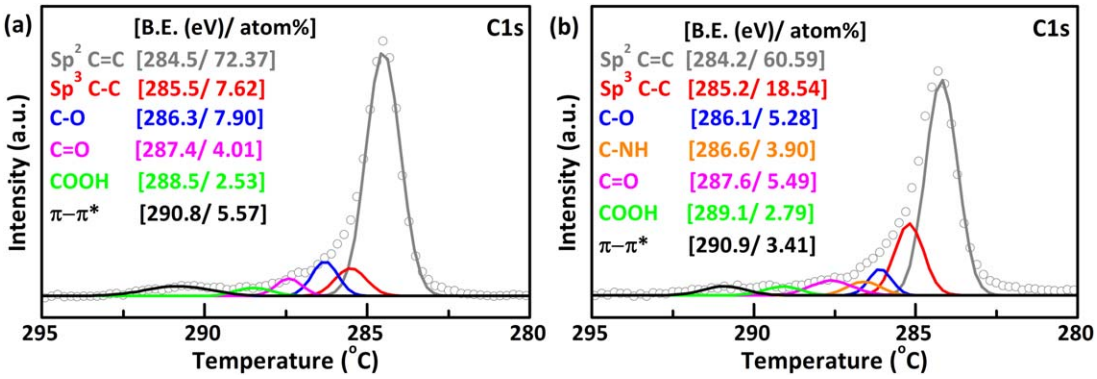

Figure 2. High-resolution XPS spectra for the C1s region of the (a) AS-MWCNTs and (b) DA-MWCNTs. [Color figure can be viewed in the online issue, which is available at wileyonlinelibrary.com.]

Nonisothermal Curing Kinetics of the MWCNT/Epoxy Composites

Nonisothermal DSC measurements with multiple βs are suggested for reliable kinetic calculations.[39] Thus, the influence of the incorporation of the AS-MWCNTs and functionalized MWCNTs on the curing reaction of the epoxy-based composites was investigated according to this technique. Figure 3 shows the DSC thermograms tested at 3, 5, 10, and 20 °C/min. The exothermic peaks shifted to higher temperatures as β increased because of the shortened reaction times with higher βs. The peak temperatures (T_ps) of all of the samples were determined, as shown in Table I. As clearly observed at lower βs, the addition of the AS-MWCNTs and DA-MWCNTs changed the shape of the curing profile. The epoxy composites reinforced with the MWCNTs showed the main exothermic peak with a small shoulder at very low temperatures. We recognized that the different functional groups established on the surface of MWCNTs induced various crosslinking mechanisms at the early state. As mentioned previously, in the AS-MWCNTs containing a small amount of oxygen-containing functionalities, a small peak appeared at a lower temperature and corresponded to esterification of hydroxyl groups. This behavior was in accordance with a literature report on the curing kinetics of epoxy/anhydride with a low proportion of hydroxyl groups.[40] Meanwhile, T_p of the EP/DA-MWCNTs visibly shifted to a lower temperature, and the shoulder peak was evident. This was mainly because, at low temperature, the amine functional groups with high nucleophilic characteristics rapidly attacked the oxygen atom to open the epoxy groups and form a secondary amine; this accelerated the curing reaction.[41]

Generally, α and $d\alpha/dt$ can be determined from nonisothermal DSC curves by means of the following expression[42–44]:

$$\alpha = \frac{\Delta H_T}{\Delta H_0} \tag{1}$$

$$\frac{d\alpha}{dt} \equiv \beta \frac{d\alpha}{dT} = \frac{1}{\Delta H_0}\left(\frac{dH}{dt}\right)_T \tag{2}$$

where ΔH_T is the heat developed at any time t during the curing reaction up to temperature T, ΔH_0 is the total heat associated with a full curing reaction, and $(dH/dt)_T$ is the instantaneous heat released at temperature T.

It is typically accepted that the most common rate of the curing reaction in thermal analysis can be described in terms of the function of temperature and the fractional conversion, as shown in the following equation[39,45]:

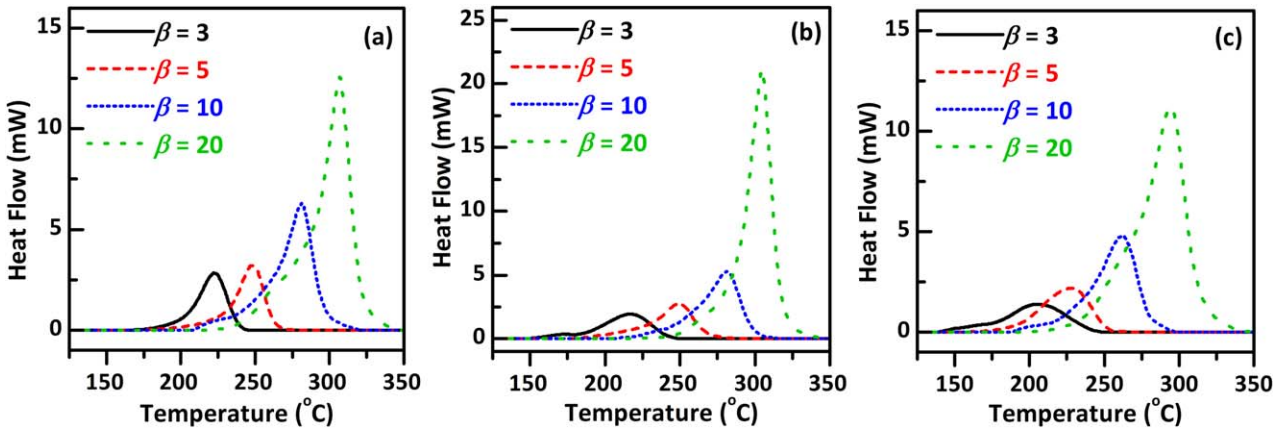

Figure 3. DSC thermograms of the (a) EP, (b) EP/AS-MWCNTs, and (c) EP/DA-MWCNTs at various βs. [Color figure can be viewed in the online issue, which is available at wileyonlinelibrary.com.]

Table I. Nonisothermal Curing Characteristics of the Epoxy Matrix and Composites at Various βs

Sample	β (°C min^{-1})	T_p (°C)	ln(β/T_p^2)	$1/T_p$	E_a
EP	3	222.81	−11.314	2.016	44.56
	5	248.37	−10.904	1.917	
	10	281.15	−10.333	1.804	
	20	306.52	−9.729	1.725	
EP/AS-MWCNTs	3	216.33	−11.288	2.043	40.78
	5	248.38	−10.904	1.917	
	10	281.09	−10.333	1.804	
	20	304.62	−9.723	1.731	
EP/DA-MWCNTs	3	205.35	−11.243	2.090	39.21
	5	227.25	−10.821	1.998	
	10	262.34	−10.264	1.867	
	20	293.70	−9.684	1.764	

$$\frac{d\alpha}{dt} = k(T)f(\alpha) \tag{3}$$

where $k(T)$ is the temperature-dependent rate constant of the reaction and $f(\alpha)$ is a function of the fractional conversion. Commonly, $k(T)$ is given by the Arrhenius equation:

$$k(T) = A\exp\left(\frac{-E_a}{RT}\right) \tag{4}$$

where A is the pre-exponential factor, E_a is the apparent activation energy, R is the universal gas constant, and T is the absolute temperature. Then, the equation of $d\alpha/dt$ can be expressed as follows:

$$\frac{d\alpha}{dt} = A\exp\left(\frac{-E_a}{RT}\right)f(\alpha) \tag{5}$$

Figure 4 shows the relationship between α and the curing temperature for the nonisothermal reaction of the polymer matrix and epoxy-based composites at different βs. With increasing β, all of the conversional curves shifted to higher temperatures. All of the systems exhibited the characteristic profile of the sigmoidal model. The curing reaction occurred slowly at relatively low temperatures; then, the reaction was accelerated remarkably as the temperature increased further. Finally, the reaction was gradually decelerated, possibly because of the reduction of reactants and the larger crosslinked networks produced; this inhibited their mobility. The conversional curves evidently differentiated at the beginning of the curing reaction (20–30% conversion), especially at a low β of 3 °C min^{-1}. The conversion was initiated at a relatively low temperature for EP/DA-MWCNTs because of the higher reactivity of the amine groups toward the epoxy groups.[41,46] For the AS-MWCNTs, the presence of hydroxyl and other oxygen-containing groups on their surface stimulated the ring opening of anhydrides and epoxides.[47,48] As a result, the progressive conversion of these systems was observed at a lower temperature than that of polymer matrix. As depicted in Figure 5, $d\alpha/dt$ gradually increased to its maximum at some intermediate value of curing conversion (α_p) and afterward gradually decreased. As shown in Table II, it was noticeable that $d\alpha/dt$ reached its maximum at a slightly lower α_p value with the incorporation of MWCNTs into the polymer matrix. This was related to the restrained mobility of the polymer chains. This was probably because of the nanostructure with the extremely high surface area and aspect ratio of the MWCNTs. Another reason for this phenomenon was the formation of larger crosslinked structures, which were induced by the surface functional groups of the MWCNTs. $d\alpha/dt$ improved with increasing β, as anticipated.

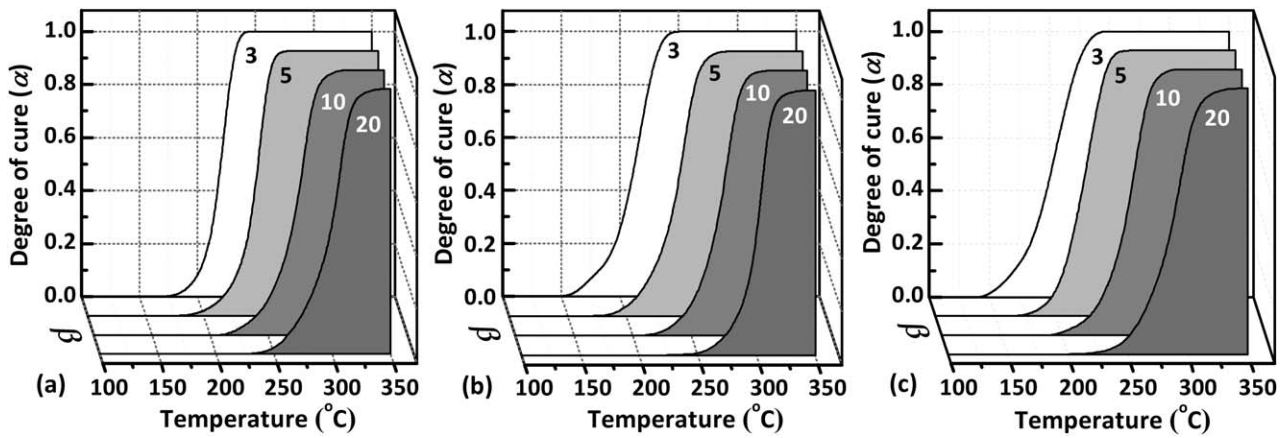

Figure 4. Dependence of the fractional conversion on the temperature for the (a) EP, (b) EP/AS-MWCNTs, and (c) EP/DA-MWCNTs at different βs.

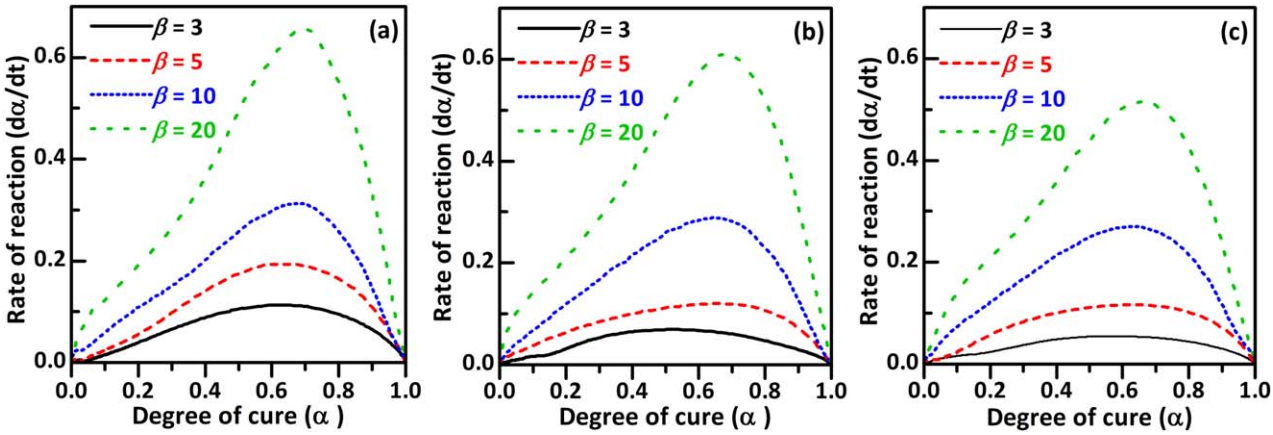

Figure 5. dα/dt as a function of the conversion for the (a) EP, (b) EP/AS-MWCNTs, and (c) EP/DA-MWCNTs at different βs. [Color figure can be viewed in the online issue, which is available at wileyonlinelibrary.com.]

To determine the appropriate kinetic model, E_a was necessary. Accordingly, the more accurate equation, often called Kissinger's equation, was used to examine the value of E_a from the nonisothermal DSC results in this work. It is given as a following equation.[49]

$$\ln \frac{\beta}{T_p^2} = \text{Constant} \frac{E_a}{RT_p} \tag{6}$$

where β is constant and T_p is from the nonisothermal DSC curve.

According to the slopes of the fitting straight lines of $\ln(\beta/T_p^2)$ against $1/T_p$, as demonstrated in Figure 6, the E_a values of all of the formulations were evaluated. The calculated values for the epoxy matrix and their composites are summarized in Table I. The E_a of epoxy matrix was 44.56 kJ/mol, whereas the E_a values of the epoxy composites decreased slightly because of the catalytic effect of the MWCNTs. The values of E_a were 40.78 and 39.21 kJ/mol for systems filled with the AS-MWCNTs and DA-MWCNTs, respectively. This was in agreement with the previous observation that the E_a decreased sharply for the resin system containing surface-treated fillers.[46,50] Thus, the AS-MWCNTs and DA-MWCNTs had catalytic effects on the initial curing process; this was also evidenced by decreased T_p.

Table II. Characteristic Peak Values of $d\alpha/dt$, $y(\alpha)$, and $z(\alpha)$ for the Epoxy Matrix and Composites at Different βs

Sample	β (°C min^{-1})	α_p	α_M	α_p^∞
EP	3	0.601	0.551	0.601
	5	0.636	0.566	0.652
	10	0.671	0.644	0.679
	20	0.700	0.673	0.700
	Mean	0.652	0.609	0.658
EP/AS-MWCNTs	3	0.595	0.478	0.642
	5	0.645	0.606	0.645
	10	0.664	0.640	0.685
	20	0.639	0.618	0.639
	Mean	0.636	0.585	0.653
EP/DA-MWCNTs	3	0.550	0.402	0.579
	5	0.610	0.418	0.628
	10	0.661	0.588	0.661
	20	0.650	0.619	0.674
	Mean	0.618	0.507	0.636

Afterward, the Málek approach was used to find the appropriate $f(\alpha)$ with the data obtained from the nonisothermal DSC measurement.[43,51,52] Two precise functions, $y(\alpha)$ and $z(\alpha)$, were constructed; these were approximated by the following equations:

$$y(\alpha) = \left(\frac{d\alpha}{dt}\right) \exp(\chi) \tag{7}$$

$$z(\alpha) = \left(\frac{d\alpha}{dt}\right) \frac{T}{\beta} \pi(\chi) \tag{8}$$

where χ is the reduced activation energy (E_a/RT) and $\pi(\chi)$ is the fourth-order rational expression of the temperature integral, as follows:[53,54]

$$\pi(\chi) = \frac{\chi^3 + 18\chi^2 + 88\chi + 96}{\chi^4 + 20\chi^3 + 120\chi^2 + 240\chi + 120} \tag{9}$$

$y(\alpha)$ and $z(\alpha)$ were normalized and plotted as a function of the conversion, as shown in Figure 7. The shape of the master

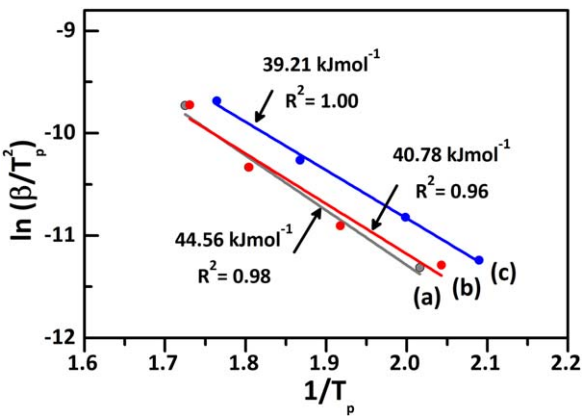

Figure 6. Kissinger plots of $\ln(\beta/T_p^2)$ versus $1/T_p$ for the (a) EP, (b) EP/AS-MWCNTs, and (c) EP/DA-MWCNTs. [Color figure can be viewed in the online issue, which is available at wileyonlinelibrary.com.]

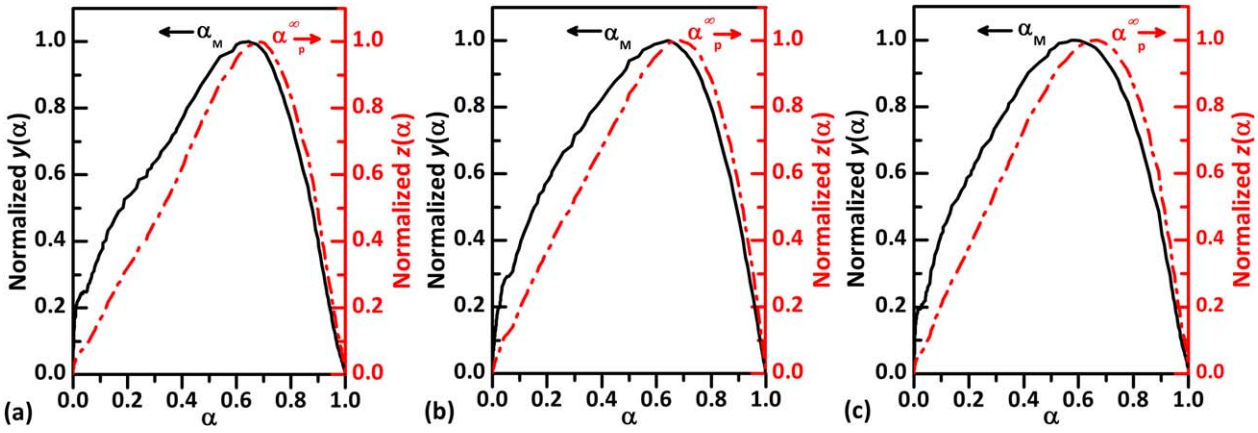

Figure 7. Normalized $y(\alpha)$ and $z(\alpha)$ values against conversion for the (a) EP, (b) EP/AS-MWCNTs, and (c) EP/DA-MWCNTs at a constant β of 10 °C/min. [Color figure can be viewed in the online issue, which is available at wileyonlinelibrary.com.]

curves was characteristic for a specific reaction model. The conversion at the maximum peak value of the normalized $y(\alpha)$ and $z(\alpha)$ curves were defined as α_M and α_p^{∞}, respectively. All of the values of α_p, α_M, and α_p^{∞} are tabulated in Table II. We observed that $0 < \alpha_M < \alpha_p^{\infty}$ and $\alpha_p^{\infty} \neq 0.632$ for all systems; thus, the two-parameter autocatalytic model, as a truncated Šesták–Berggren (SB) model or SB(m,n) equation, was more suitable for elucidating the curing kinetics.[42,44] This empirical model is provided in the following equation:

$$f(\alpha) = (1\text{-}\alpha)^n \tag{10}$$

Rewriting eq. (5) with the SB(m,n) function gives

$$\frac{d\alpha}{dt} = A \exp(-\chi)\alpha^m(1-\alpha)^n \tag{11}$$

where m and n are kinetic parameters. Taking the natural logarithm on both sides of eq. (11) and rearranging yields

$$\ln\left[\left(\frac{d\alpha}{dt}\right)\exp(\chi)\right] = \ln A + n\ln\left[\alpha^{m/n}(1-\alpha)\right] \tag{12}$$

where

$$\alpha_M = \frac{m}{m+n} \tag{13}$$

n could be estimated from the slope of eq. (12). Then, the m value could be calculated from eq. (13). m, n, and ln A obtained from the SB(m,n) model of the epoxy–anhydride systems filled with AS-MWCNTs and functionalized MWCNTs are summarized in Table III. The overall reaction orders were 3.032, 2.956, and 2.206 for the EP, EP/AS-MWCNTs, and EP/DA-MWCNTs, respectively. The m value tended to decrease in the order EP < EP/AS-MWCNTs < EP/DA-MWCNTs, whereas the n value changed slightly. The small amount of hydroxyl groups and oxygen-containing groups on the AS-MWCNTs accelerated the curing mechanism at the early stage; however, no effect was observed on the overall reaction. Meanwhile, the reaction orders were reduced remarkably by the addition of DA-MWCNTs into the systems; this might have been due to the steric hindrance of crosslinked networks generated via reactive amino functional groups from the nanotube surface in the early steps of the curing reaction; this restricted the mobility of the reactive molecules.[55]

Dispersion of the MWCNTs in the Epoxy Nanocomposites

The degree of dispersion of the CNTs in the polymer matrix strongly influenced the mechanical and thermal properties and the thermal and electrical conductivities of the polymer nanocomposites. The SEM images in Figure 8 illustrate the dispersion of the AS-MWCNTs and DA-MWCNTs in the cryofractured surfaces of the epoxy nanocomposites. Although the AS-MWCNTs had the oxygen-functionalities, which could interact with the epoxy matrix, the entangled AS-MWCNT bundles were obvious. On the contrary, the DA-MWCNTs were well dispersed in the nanocomposites as a result of the improved interfacial interactions between the benzoyl moieties of the DA-MWCNTs and the epoxy matrix.

Dynamic Mechanical Properties of the MWCNT/Epoxy Composites

The storage moduli E' and loss moduli E'' of the epoxy composites recorded at 1-Hz frequency are illustrated in Figure 9. The

Table III. Calculated Kinetic Parameters from the SB(m,n) Model for the Epoxy Matrix and Composites at Different βs

Sample	β (°C min^{-1})	m	n	ln A
EP	3	1.028	0.838	9.972
	5	1.252	0.958	10.222
	10	2.441	1.352	11.370
	20	2.867	1.392	11.480
	Mean	1.897	1.135	10.761
EP/AS-MWCNTs	3	1.300	0.884	8.806
	5	1.808	1.175	9.445
	10	1.958	1.101	9.628
	20	2.222	1.374	10.719
	Mean	1.822	1.134	9.650
EP/DA-MWCNTs	3	0.546	0.812	8.013
	5	0.530	0.738	8.329
	10	1.604	1.126	9.441
	20	2.149	1.322	9.953
	Mean	1.207	0.999	8.934

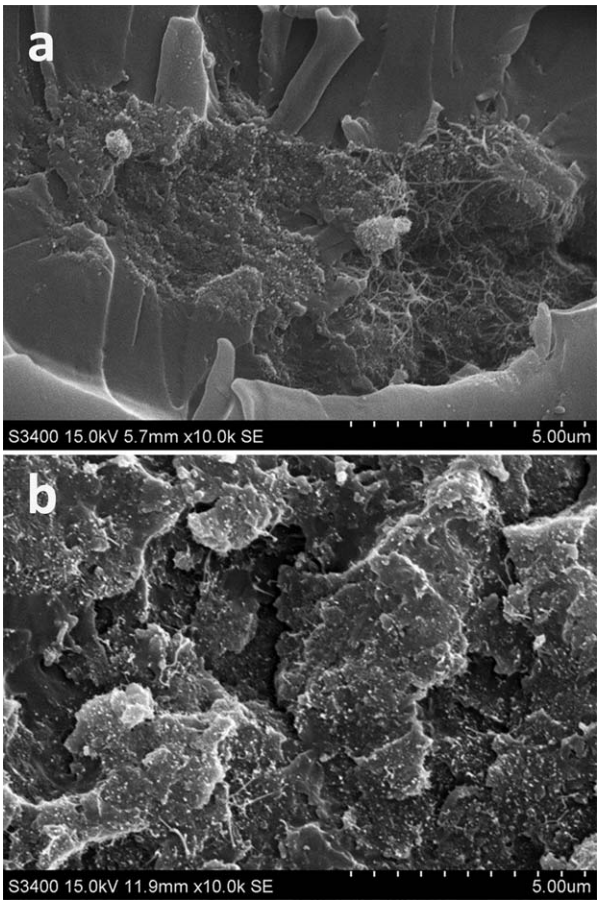

Figure 8. SEM images of the cryofractured surfaces of the epoxy nanocomposites containing the (a) AS-MWCNTs and (b) DA-MWCNTs.

storage modulus at room temperature of the epoxy resin without the MWCNTs (EP) was approximately 1.56 GPa. The storage moduli in the glassy state increased to 2.42 and 2.64 GPa with addition of 0.3 wt % AS-MWCNTs and DA-MWCNTs, respectively, as a result of the reinforcing effect of the CNTs. This result was in agreement with the work done by Montazeri *et al.*,[56] who investigated the viscoelastic properties of the epoxy composites containing untreated MWCNTs. They reported that the glassy storage modulus was enhanced as a function of the MWCNT loading and eventually dropped at loadings higher than 0.5 wt % because of the agglomeration of MWCNTs. The surface functionality also affected the mechanical properties of the composites. Namely, the oxygen-containing groups on the AS-MWCNTs and the amino groups on the DA-MWCNTs decreased the van der Waals forces among the nanotubes and possibly reacted with the epoxide ring of EP via a ring-opening reaction; this led to improved interfacial adhesion and better load transfer between the MWCNTs and the epoxy matrix. Because the amino groups were more reactive toward nucleophilic addition in the curing reaction than the hydroxyl or carboxyl groups, the crosslinking reaction in the EP/DA-MWCNTs was significantly pronounced in comparison with that in the EP/AS-MWCNTs; this resulted in stronger interfacial interaction and higher mechanical properties in the EP/DA-MWCNTs. Salam *et al.*[57] also reported a similar trend, in which epoxy nanocomposites containing 0.2 wt % MWCNTs treated with amino and carboxyl groups showed an improvement in the glassy storage modulus of about 47% in comparison with the neat epoxy. A slight increase in the storage modulus in the rubbery plateau region, which principally refers to the crosslink density in the polymer matrix, for EP/DA-MWCNTs confirmed the promoted crosslinking reaction in the epoxy matrix. According to our previous study,[30] we found that the crosslink densities of the EP, EP/AS-MWCNTs, and EP/DA-MWCNTs were approximately 5.1, 5.3, and 5.8 mmol m^{-1}, respectively.

The glass-transition temperature (T_g) was investigated from the maximum value at the peak of the loss modulus curve; this corresponded to the initial drop from the glassy state into the rubbery state. The change in the glass transition was attributed to the increase in the molecular mobility when the molecular chain obtained adequate energy to overcome the configurational rearrangements of the polymer chain backbones. The results reveal that the loss modulus peak shifted to a higher temperature with the values ranging from 131 °C in the epoxy matrix to 134 °C in the EP/AS-MWCNTs and 136 °C in the EP/DA-MWCNTs. It is well known that T_g of materials involved the mobility of the polymer chain or free volume fraction. The addition of MWCNTs possibly hindered the chain mobility of the matrix and reduced the free volume fraction; this resulted in the enhancement of T_g.

Thermal Conductivity of the MWCNT/Epoxy Composites

To enhance the ability of heat dissipation for the polymer composites, intrinsic thermally conductive fillers with extremely high aspect ratios were often used. As shown in previous publications, the MWCNTs at low filler loadings exhibited high performance in the formation of heat-conductive pathways along the matrix because of their characteristic aspect. However, the surface functional groups intensively affected the formation of effective heat-conductive pathways. Hence, thermal conductivity of the MWCNTs/epoxy composites with various functional groups was calculated as follows:

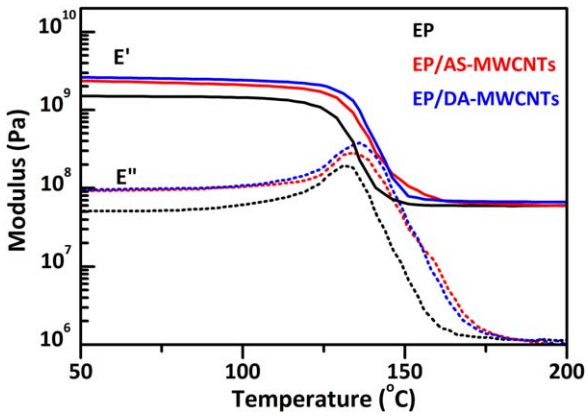

Figure 9. Dynamic mechanical properties (storage moduli E' and loss moduli E'') of the matrix and composites at a frequency of 1 Hz. [Color figure can be viewed in the online issue, which is available at wileyonlinelibrary.com.]

Table IV. Thermal Conductivity for the Epoxy Matrix and Composites

Sample	α ($mm^2\ s^{-1}$)	ρ ($g\ cm^{-3}$)	C_p ($J\ g^{-1}\ °C^{-1}$)	K ($W\ m^{-1}\ K^{-1}$)	K_R (%)[a]
EP	0.108	1.1825	1.229	0.157	100
EP/AS-MWCNTs	0.116	1.1866	1.369	0.182	116
EP/DA-MWCNTs	0.118	1.1838	1.381	0.193	123

[a] K_R, relative thermal conductivity of composites ($K_{composite} \times 100/K_{matrix}$), where K_{matrix} is thermal conductivity of EP and $K_{composite}$ is thermal conductivity of epoxy composites filled AS-MWCNTs and DA-MWCNTs.

$$K = \alpha \rho C_p \quad (14)$$

where K is the thermal conductivity of the composites, α is the thermal diffusivity, and ρ is the density.

The thermal conductivity of the cured epoxy and epoxy/MWCNT composites is summarized in Table IV. The thermal conductivity values were 0.193, 0.182, and 0.157 $W\ m^{-1}\ K^{-1}$ for the EP/AS-MWCNTs, EP/DA-MWCNTs, and EP, respectively. In theory, the strong covalent bonding between the carbon atoms of the tubes and the matrix as a result of the surface functionalization of MWCNTs could act as the scattering center for thermal energy carriers, increasing the boundary scattering losses and thus decreasing the thermal conductivity. With molecular dynamics simulations, Fadgett and Brenner[58] predicted that the chemical attachment of 1% of the carbon atoms on a pristine single-walled CNT surface with phenyl rings decreased its intrinsic thermal conductivity by greater than a factor of 3. However, the EP/DA-MWCNTs showed a higher thermal conductivity than the EP/AS-MWCNTs; this could be explained in terms of the difference in the reactivity of the functional groups existing on the nanotubes. The amino groups established on the DA-MWCNTs effectively reacted with the epoxy rings of EP; this led to an improvement in the interfacial heat transport between the epoxy matrix and the MWCNTs as well as a good dispersion of MWCNTs in the matrix for better continuity of the heat-conductive pathway. In contrast, the oxygen-containing functional groups on the nonfunctionalized MWCNTs could only induce the ring-opening addition of the curing reaction; this resulted in weak interfacial interactions and the formation of a looser crosslinked network. Therefore, the EP/DA-MWCNTs provided a higher thermal conductivity than the EP/AS-MWCNTs; this is generally related to a high thermal dissipation. Also, this result implied that the enhanced heat transport at the interface and the dispersability of the MWCNTs in the matrix were the dominant factors facilitating the transfer of thermal energy across the matrix–MWCNT interface. This was in agreement with the results of previous studies by Yang *et al.*[38] and Khare *et al.*,[59] who studied epoxy composites containing CNTs grafted with triethylene tetraamine and amido–amine groups, respectively.

CONCLUSIONS

XPS analysis was applied to distinguish the chemical compositions of the uppermost surface of the AS-MWCNTs and DA-MWCNTs. This result revealed that there was a small number of oxygen-containing groups established even on the surface of the unmodified sample. The N1s peak was observed only in the XPS survey spectrum of the DA-MWCNTs at about 400.2 eV and was attributed to the primary amine bonded with C═C bond; this indicated the effective grafting of diaminobenzoyl moieties on their surface via a direct Friedel–Crafts acylation in a mild PPA/P_2O_5 medium. According to nonisothermal DSC analysis, the reactive functional groups present on the surfaces of the AS-MWCNTs and DA-MWCNTs accelerated the nucleophilic addition reaction of the epoxy composites. This induced decreases in the exothermic T_p and the activation energy. Differences in the fractional conversion and $d\alpha/dt$ of the curing process were evident, remarkably, at the early stage. Additionally, the Málek approach revealed that the two-parameter autocatalytic model, as a truncated SB model, was more suitable for elucidating the curing kinetics. It was noticeable that $d\alpha/dt$ reached its maximum at lower α_p values for the MWCNT-incorporated epoxy composites. The reaction orders were also reduced by the addition of MWCNTs into the systems. Furthermore, it was found that DA-MWCNTs were well dispersed in the epoxy composites in comparison with AS-MWCNTS owing to the presence of reactive diaminobenzoyl moieties. The DA-MWCNTs acheived better interfacial interactions between the nanotubes and the matrix and a higher crosslink density; this, thereby, provided more effective load transfer and heat-conductive pathways. The epoxy composite modified with DA-MWCNTs thus presented a higher T_g and a higher thermal conductivity; this resulted in the enhancement of heat dissipation.

ACKNOWLEDGMENTS

This research was supported by the Rachadapisek Sompote Fund for Postdoctoral Fellowships of Chulalongkorn University and the Thailand Research Fund (institutional research grant 5780014). The authors sincerely thank Mektec Manufacturing Corp. (Thailand), Ltd., for the supporting materials, analytical instruments, and kind assistance.

REFERENCES

1. Petrie, E. M. Epoxy Adhesive Formulations; McGraw-Hill: New York, **2005**.
2. Zhou, T.; Wang, X.; Mingyuan, G. U.; Liu, X. *Polymer* **2008**, *49*, 4666.
3. Gu, J. W.; Zhang, Q. Y.; Dang, J.; Xie, C. *Polym. Adv. Technol.* **2012**, *23*, 1025.

4. Zhu, B. L.; Ma, J.; Wu, J.; Yung, K. C.; Xie, C. S. *J. Appl. Polym. Sci.* **2010**, *118*, 2754.
5. Li, S. S.; Qi, S. H.; Liu, N. L.; Cao, P. *Thermochim. Acta* **2011**, *523*, 111.
6. Yu, H.; Li, L. L.; Kido, T.; Xi, G. N.; Xu, G. C.; Guo, F. *J. Appl. Polym. Sci.* **2012**, *124*, 669.
7. Njuguna, J.; Pielichowski, K.; Alcock, J. R. *Adv. Eng. Mater.* **2007**, *9*, 835.
8. Han, M. S.; Lee, Y. K.; Kim, W. N.; Lee, H. S.; Joo, J. S.; Park, M.; Lee, H. J.; Park, C. R. *Macromol. Res.* **2009**, *17*, 863.
9. Wu, A. S.; Chou, T. W. *Mater. Today* **2012**, *15*, 302.
10. Shearer, C. J.; Cherevan, A.; Eder, D. *Adv. Mater.* **2014**, *26*, 2295.
11. Qian, D.; Wagner, G. J.; Liu, W. K.; Yu, M. F.; Ruoff, R. S. *Appl. Mech. Rev.* **2002**, *55*, 495.
12. Volder, M. F. L. D.; Tawfick, S. H.; Baughman, R. H.; Hart, A. J. *Science* **2013**, *339*, 535.
13. Zhang, Q.; Huang, J. Q.; Qian, W. Z.; Zhang, Y. Y.; Wei, F. *Small* **2013**, *9*, 1237.
14. Liu, S.; Chen, F.; Zhang, Y.; Shen, Q.; Huang, Z.; Zhang, L. *Polym. Compos.* **2014**, *35*, 548.
15. Roy, D.; Tiwari, N.; Mukhopadhyay, K.; Saxena, A. K. *Polymer* **2014**, *55*, 583.
16. Wang, B.; Yin, J.; Wang, L.; Gao, Y. *Macromol. Mater. Eng.* **2014**, *299*, 344.
17. Theodore, M.; Hosur, M.; Thomas, J.; Jeelani, S. *Mater. Sci. Eng. A* **2011**, *528*, 1192.
18. Star, A.; Stoddart, J. F.; Steuerman, D.; Diehl, M.; Boukai, A.; Wong, E. W.; Yang, X.; Chung, S. W.; Choi, H.; Heath, J. R. *Angew. Chem. Int. Ed.* **2001**, *40*, 1721.
19. Vaisman, L.; Wagner, H. D.; Marom, G. *Adv. Colloid Interface Sci.* **2006**, *128*, 37.
20. Wepasnick, K. A.; Smith, B. A.; Schrote, K. E.; Wilson, H. K.; Diegelmann, S. R.; Fairbrother, D. H. *Carbon* **2011**, *49*, 24.
21. Lee, H. J.; Han, S. W.; Kwon, Y. D.; Tan, L. S.; Baek, J. B. *Carbon* **2008**, *46*, 1850.
22. Han, S. W.; Oh, S. J.; Tan, L. S.; Baek, J. B. *Carbon* **2008**, *46*, 1841.
23. Yang, S. Y.; Ma, C. C. M.; Teng, C. C.; Huang, Y. W.; Liao, S. H.; Huang, Y. L.; Tien, H. W.; Lee, T. M.; Chiou, K. C. *Carbon* **2010**, *48*, 592.
24. Li, N.; Liu, H.; Zhang, Z. *Polym. Compos.* **2014**, *35*, 1275.
25. Zhang, P.; Qui, D.; Chen, H.; Sun, J.; Wang, J.; Qin, C.; Dai, L. *J. Mater. Chem. A* **2015**, *3*, 1442.
26. Kim, K. S.; Jeon, I. Y.; Ahn, S. N.; Kwon, Y. D.; Baek, J. B. *J. Mater. Chem.* **2011**, *21*, 7337.
27. Wang, D. H.; Tan, L. S.; Huang, H.; Dai, L.; Osawa, E. *Macromolecules* **2008**, *42*, 114.
28. Lim, D. H.; Lyons, C. B.; Tan, L. S.; Baek, J. B. *J. Phys. Chem.* **2008**, *112*, 12188.
29. Pongsa, U.; Samthong, C.; Somwangthanaroj, A. *Polym. Eng. Sci.* **2013**, *53*, 2194.
30. Pongsa, U.; Somwangthanaroj, A. *J. Appl. Polym. Sci.* **2013**, *130*, 3184.
31. Chen, W.; Qian, X. M.; He, X. Q.; Liu, Z. Y.; Liu, J. P. *J. Appl. Polym. Sci.* **2012**, *123*, 1983.
32. Kundu, S.; Wang, Y.; Xia, W.; Muhler, M. *J. Phys. Chem. C* **2008**, *112*, 16869.
33. Hou, P. X.; Liu, C.; Cheng, H. M. *Carbon* **2008**, *46*, 2003.
34. Ruelle, B.; Felten, A.; Ghijsen, J.; Drube, W.; Johnson, R. L.; Liang, D.; Erni, R.; Van Tendeloo, G.; Sophie, P.; Dubois, P.; Godfriod, M.; Hecq, M.; Bittencourt, C. *Micron* **2009**, *40*, 85.
35. Coates, M.; Nyokong, T. *Int. J. Nanosci.* **2013**, *12*, 1350017.
36. Okpalugo, T. I. T.; Papakonstantinou, P.; Murphy, H.; McLaughlin, J.; Brown, N. M. D. *Carbon* **2005**, *43*, 153.
37. Koysuren, O.; Karaman, M.; Ozyurt, D. *J. Appl. Polym. Sci.* **2013**, *127*, 4557.
38. Yang, K.; Gu, M.; Guo, Y.; Pan, X.; Mu, G. *Carbon* **2009**, *47*, 1723.
39. Vyazovkin, S.; Burnham, A. K.; Criado, J. M.; Perez-Maqueda, L. A.; Popescu, C.; Sbirrazzuoli, N. *Thermochim. Acta* **2011**, *520*, 1.
40. Foix, D.; Yu, Y.; Serra, A.; Ramis, X.; Salla, J. M. *Eur. Polym. J.* **2009**, *45*, 1454.
41. Vyazovkin, S.; Sbirrazzuoli, N. *Macromolecules* **1996**, *29*, 1867.
42. Fan, M.; Liu, J.; Li, X.; Cheng, J.; Zhang, J. *Thermochim. Acta* **2013**, *554*, 39.
43. Málek, J. *Thermochim. Acta* **1992**, *200*, 257.
44. Šesták, J.; Berggren, G. *Thermochim. Acta* **1971**, *3*, 1.
45. Ventura, I. A.; Rahaman, A.; Lubineau, G. *J. Appl. Polym. Sci.* **2013**, *130*, 2722.
46. Zhou, X. W. T.; Liu, X. H.; Lai, J. Z. *eXPRESS Polym. Lett.* **2010**, *4*, 217.
47. Fernandez-Francos, X.; Ramis, X.; Serra, A. *J. Polym. Sci. Part A: Polym. Chem.* **2014**, *52*, 61.
48. Mohan, P. *Polym.-Plast. Technol.* **2013**, *52*, 107.
49. Kissinger, H. E. *Anal. Chem.* **1957**, *29*, 1702.
50. Harsch, M.; Karger-Kocsis, J.; Holst, M. *Eur. Polym. J.* **2007**, *43*, 1168.
51. Zhou, Z.; Li, A.; Bai, R.; Sun, J. *Polym. Compos.* **2014**, *35*, 596.
52. Málek, J. *Thermochim. Acta* **1989**, *138*, 337.
53. Senum, G. I.; Yang, R. T. *J. Therm. Anal.* **1977**, *11*, 445.
54. Zabihi, O.; Aghaie, M.; Zare, K. *J. Therm. Anal. Calorim.* **2013**, *111*, 703.
55. Wan, J.; Bu, Z. Y.; Xu, C. J.; Li, B. G.; Fan, H. *Thermochim. Acta* **2011**, *519*, 72.
56. Montazeri, A.; Pourshamsian, K.; Riazian, M. *Mater. Des.* **2012**, *36*, 408.
57. Salam, M. B. A.; Hosur, M. V.; Zainuddin, S.; Jeelani, S. *Open J. Compos. Mater.* **2013**, 3, 1.
58. Fadgett, C. W.; Brenner, D. W. *Nano Lett.* **2004**, *4*, 1051.
59. Khare, K. S.; Khabaz, F.; Khare, R. *ACS Appl. Mater. Interfaces* **2014**, *6*, 6098.